

See discussions, stats, and author profiles for this publication at: <https://www.researchgate.net/publication/272272319>

One-Pot Synthesis of Fe₂O₃ Nanoparticles on Nitrogen-Doped Graphene as Advanced Supercapacitor Electrode Materials

ARTICLE *in* THE JOURNAL OF PHYSICAL CHEMISTRY C · AUGUST 2014

Impact Factor: 4.77 · DOI: 10.1021/jp502226j

CITATIONS

28

READS

20

5 AUTHORS, INCLUDING:



Zhaoling Ma

Hunan University

14 PUBLICATIONS 115 CITATIONS

SEE PROFILE

One-Pot Synthesis of Fe_2O_3 Nanoparticles on Nitrogen-Doped Graphene as Advanced Supercapacitor Electrode Materials

Zhaoling Ma,[†] Xiaobing Huang,[‡] Shuo Dou,[†] Jianghong Wu,[†] and Shuangyin Wang^{*,†,§}

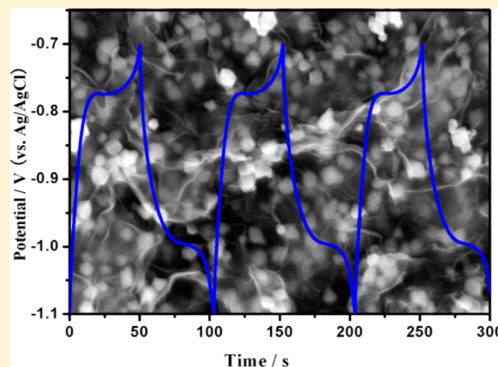
[†]State Key Laboratory of Chem/Bio-Sensing and Chemometrics, College of Chemistry and Chemical Engineering, Hunan University, Changsha 410082, People's Republic of China

[‡]College of Chemistry and Chemical Engineering, Hunan University of Arts and Science, Changde, Hunan Province, People's Republic of China

[§]School of Physics and Astronomy, The University of Manchester, Oxford Road, Great Manchester M139PL, United Kingdom

Supporting Information

ABSTRACT: Fe_2O_3 supported on nitrogen-doped graphene ($\text{Fe}_2\text{O}_3/\text{N-rGO}$) hydrogel was prepared by a facial one-pot hydrothermal method. The efficient Fe_2O_3 loading and nitrogen doping of graphene was realized with this method. The morphology and structure of the samples were characterized by scanning electron microscopy, high-resolution transmission electron microscopy, thermal gravimetric analysis, Raman spectra, X-ray diffraction, and nitrogen isothermal adsorption–desorption. The chemical environment of the surface composition of the samples was recorded by X-ray photoelectron spectroscopy. The electrochemical performance was tested with a three-electrode system in the aqueous electrolyte of 1 M KOH. The electrochemical measurement demonstrated that $\text{Fe}_2\text{O}_3/\text{N-rGO}$ shows a specific capacitance as high as 618 F g^{-1} at a discharge current density of 0.5 A g^{-1} . Even at the current density of 10 A g^{-1} , the specific capacitance is still as high as 350 F g^{-1} . After 5000 cycles, the capacity retention is still maintained at 56.7%.



INTRODUCTION

Supercapacitors are considered as a promising candidate for energy storage due to its combinative advantages of the electrical double-layer capacitor (EDLC) and pseudocapacitor.¹ In recent years, due to the significant advantages of supercapacitors that the high energy and long cycle life can be released in short time and remain, supercapacitors have attracted much attention, particularly in respect of portable electronic devices.^{2,3} Graphene as a new member of carbon materials with high theoretical specific surface area ($2620 \text{ m}^2 \text{ g}^{-1}$), good electrical conductivity,⁴ and two-dimensional (2D) structure is well suitable as the support material of redox species such as metal oxides NiO , Ni(OH)_2 , MnO_2 , In_2O_3 , RuO_2 , and so forth.^{5–10} The metal oxide/graphene composites perfectly show the synergistic effects of EDLC from graphene and faradaic pseudocapacitance from metal oxides.

Up to now, various methods have been developed to hybridize transition-metal oxide nanoparticles onto graphene. Among various synthesis methods, the metal oxide/graphene composite prepared through the hydrothermal reduction of metal salts and graphene oxide (GO) is widely used, owing to the simple operation and the low cost. Moreover, the three-dimensional (3D) graphene hydrogel as a metal oxide support can offer the supporting network for anchoring metal oxide nanoparticles. That is in favor of largely improving the electrical conductivity of metal oxides and the specific surface area of the electrodes. On the other hand, the heteroatom doping of

graphene as an electrode material or/and the support of the electrode materials has been demonstrated to be an efficient way to improve the performance of the hybrid composites for electrocatalysis and energy storage. The heteroatom doping does not only contribute to additional pseudocapacitance and to increasing the double-layer electrical capacitance of graphene^{11,12} but also enhances the interaction between metal oxide or metal nanoparticles and graphene to improve the electrochemical stability of the composites.

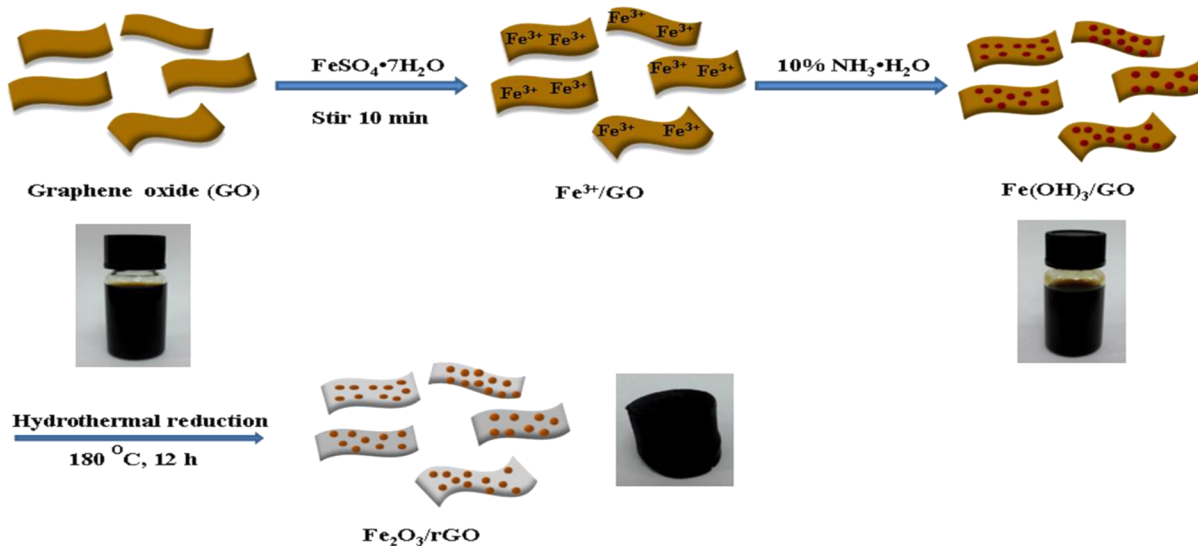
Fe_2O_3 with the advantages of low cost and environmental harmlessness has high theoretical specific capacitance.^{13,14} However, during their synthesis, metal oxides are usually easy to aggregate and to grow into large particles that lose their dispersion and hinder good synergistic effects. Herein, we developed a facial one-pot synthetic method to prepare Fe_2O_3 nanoparticles supported on nitrogen-doped graphene ($\text{Fe}_2\text{O}_3/\text{N-rGO}$) by using the oxidation ability of GO for Fe^{2+} ¹⁵ and subsequent hydrothermal nitrogen doping. In this simple process, the formation and deposition of Fe_2O_3 nanoparticles and the nitrogen doping were realized. Homodispersed hematite (Fe_2O_3) nanoparticles were successfully anchored on the surface of N-rGO by controlling the growth rate of nanoparticles and the quantity of added Fe^{2+} . The electro-

Received: March 4, 2014

Revised: July 2, 2014

Published: July 8, 2014



Scheme 1. Illustration of the Synthesis of the $\text{Fe}_2\text{O}_3/\text{N-rGO}$ Hydrogel

chemical characterizations demonstrated that the as-obtained $\text{Fe}_2\text{O}_3/\text{N-rGO}$ shows high specific capacitance with good stability.

EXPERIMENTAL DETAILS

Preparation of Graphite Oxide. Graphite oxide was prepared according to a modified Hummers method. Briefly, graphite powders (5.0 g) (350 mesh) and sodium nitrates (5.0 g) were added into concentrated sulfuric acid (115 mL) before the mixture was kept in an ice bath for 1 h under gentle agitation. The temperature of the mixture was kept to below 5 $^\circ\text{C}$. Potassium permanganate (15.0 g) was added stepwise and kept the system temperature lower than 40 $^\circ\text{C}$ after the ice bath was removed. Then, the mixture was heated to 40 $^\circ\text{C}$ and kept for 45 min. The ultrapure water (140 mL) was added, and the temperature of the solution was kept at 98 $^\circ\text{C}$ for another 45 min. The mixture turned from brown to yellow, and another copious 350 mL of water was added. Finally, 30 mL of H_2O_2 (30% v/v solution) was slowly added when the temperature decreased to 60 $^\circ\text{C}$. The mixture was centrifuged and washed with HCl solution (5%) three times followed by water several times until the pH of the system was about 7. The resulting sample was dried in a vacuum oven at 60 $^\circ\text{C}$ for 72 h.

Preparation of $\text{Fe}_2\text{O}_3/\text{N-rGO}$ Hydrogel, N-Doped rGO (N-rGO) Hydrogel, and Reduced Graphene Oxide Hydrogel (rGO). $\text{Fe}_2\text{O}_3/\text{N-rGO}$ hydrogel was prepared by the following process. Briefly, 250 mg of graphite oxide was dispersed in 108 mL of H_2O and sonicated with probe sonication for 10 min. The resulting suspension was subjected to centrifugation at 5000 rpm for 10 min, and the as-obtained GO suspension was divided into two groups for later use. Then, 120 or 200 mg of $\text{FeSO}_4 \cdot 7\text{H}_2\text{O}$ was added into 54 mL of a 2 mol L^{-1} GO suspension followed by intense agitation for 10 min. Then, 6 mL of $\text{NH}_3 \cdot \text{H}_2\text{O}$ (30%) was added dropwise for 30 min, and then, the as-obtained brown viscous suspension was transferred into a stainless steel vessel and subjected to the hydrothermal reduction at 180 $^\circ\text{C}$ for 12 h. Afterward, a cylinder hydrogel of $\text{Fe}_2\text{O}_3/\text{N-rGO}$ was formed and then dialyzed against ultrapure water (18.2 M Ω) to remove the residual. The two $\text{Fe}_2\text{O}_3/\text{N-rGO}$ hydrogels with different $\text{FeSO}_4 \cdot 7\text{H}_2\text{O}$ masses added into the reaction system are defined

as $\text{Fe}_2\text{O}_3/\text{N-rGO-1}$ (120 mg, $\text{FeSO}_4 \cdot 7\text{H}_2\text{O}$) and $\text{Fe}_2\text{O}_3/\text{N-rGO-2}$ (200 mg, $\text{FeSO}_4 \cdot 7\text{H}_2\text{O}$). For comparison, N-rGO was also prepared under the similar conditions in the absence of $\text{FeSO}_4 \cdot 7\text{H}_2\text{O}$. The rGO was prepared by a similar method in the absence of $\text{FeSO}_4 \cdot 7\text{H}_2\text{O}$ and ammonia.

Characterizations. The morphologies of the samples were studied by a scanning electron microscope (SEM, Hitachi, S-4800) and a transmission electron microscope (TEM, JEOL, JEM-2010). Raman spectroscopy was performed on a Jobin Yvon Labram-010 micro-Raman system with a 632 nm laser excitation. X-ray diffraction (XRD) analyses were executed on a Siemens D500 diffractometer with a $\text{Cu K}\alpha$ source (1.54056 Å). X-ray photoelectron spectroscopy (XPS) was recorded on a ThermoFisher-VG Scientific (ESCALAB 250Xi) photoelectron spectrometer. Thermal gravimetric analysis was executed with a NETZSH STA 449C analyzer at a heating rate of 10 $^\circ\text{C}/\text{min}$ under an air atmosphere. The Brunauer–Emmett–Teller (BET) specific surface area and porous structure characteristics of the samples were probed by a nitrogen adsorption–desorption method at 77 K (SSA-4200).

Electrochemical Measurement. Cyclic voltammetry (CV) and galvanostatic charge/discharge of the samples were carried out in a three-electrode cell system using 1 M KOH aqueous solution as the electrolyte by a CHI 760E electrochemical workstation (CH Instruments Inc.). Platinum mesh (1 cm \times 1 cm) and a Ag/AgCl electrode were used as the counter electrode and reference electrode, respectively. The working electrode was prepared as follows: $\text{Fe}_2\text{O}_3/\text{N-rGO}$ hydrogel was dispersed in 5 mL of ultrapure water (18.2 M Ω) and underwent ultrasonication with a 300 W ultrasonic instrument for 1 h; 20 μL of the suspension and 5 μL of Nafion solution (0.05% Nafion in ethyl alcohol) were in sequence dropped onto a glassy carbon electrode (ϕ 5 mm). The mass of active material (m) on the glassy carbon electrode was calculated using the following equation

$$m = \frac{m_h \times w\% \times 20}{5000} \quad (1)$$

where m_h is the mass of the hydrogel and $w\%$ is the mass fraction of the active material of the hydrogels.

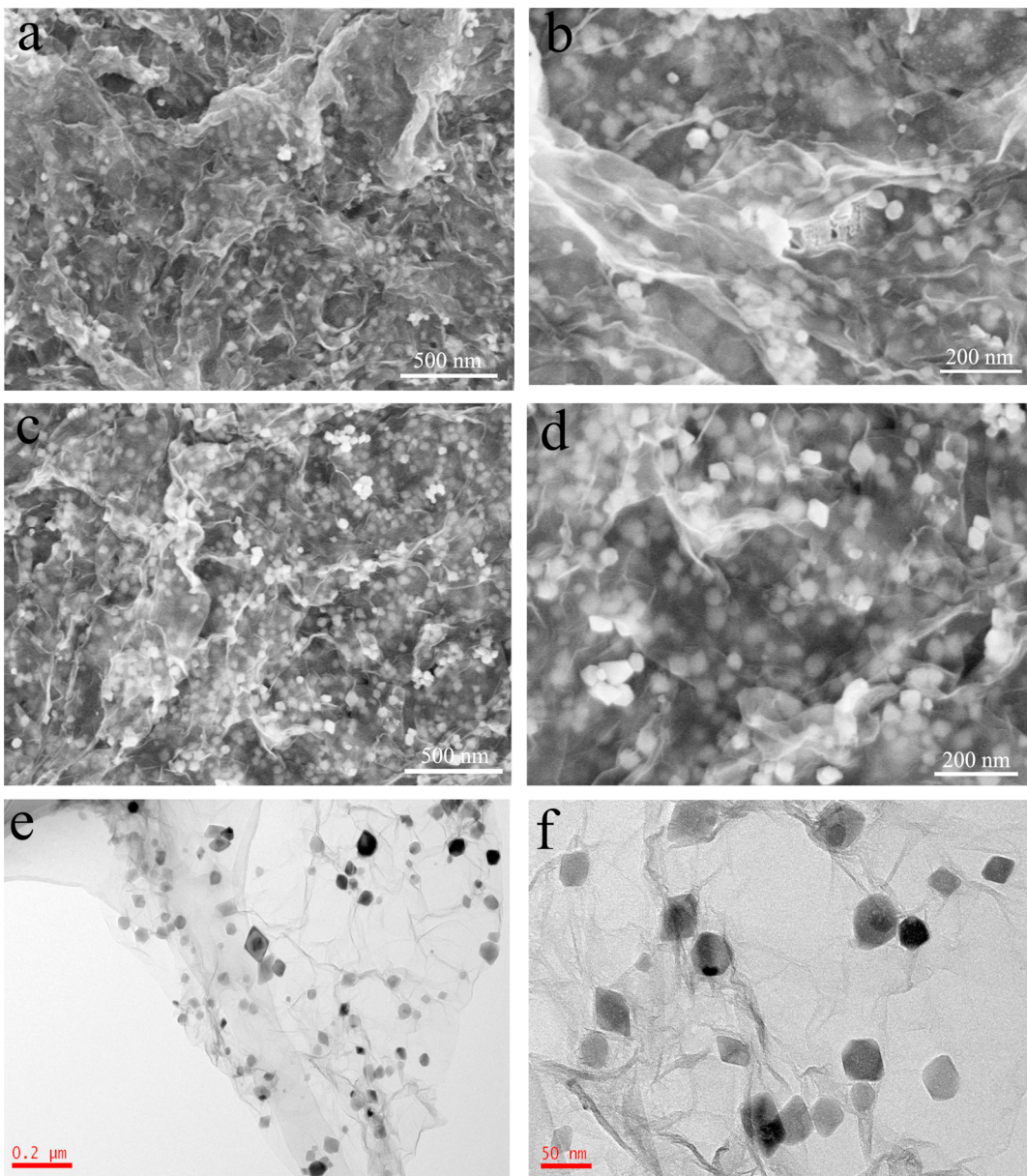


Figure 1. (a), (b) SEM image of the $\text{Fe}_2\text{O}_3/\text{N-rGO-1}$. (c,d) SEM image of the $\text{Fe}_2\text{O}_3/\text{N-rGO-2}$. (e,f) TEM image of the $\text{Fe}_2\text{O}_3/\text{N-rGO}$ composites.

The specific capacitance was calculated from the galvanostatic charge/discharge curves using the following equation

$$C_s = \frac{I\Delta t}{m\Delta V} \quad (2)$$

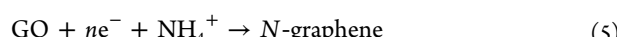
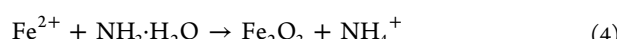
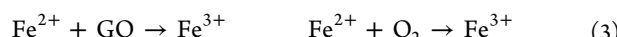
where I is the discharge current, Δt is the time for a full discharge, m is the mass of the active material, and ΔV is the voltage change after a full discharge.

All of the electrochemical impedance spectra were measured at open-circuit voltage on Autolab PGSTAT302N (Metrohm-Autolab BV, Utrecht, The Netherlands) over the frequency range from 100 kHz to 10 mHz at an amplitude of 5 mV.

RESULTS AND DISCUSSION

The processes of the synthesis of $\text{Fe}_2\text{O}_3/\text{N-rGO}$ hydrogels are shown in Scheme 1. GO was obtained by the probe ultrasonication of graphite oxide. In the stirring process, Fe^{2+} was uniformly dispersed on the surface of the GO with the

assistance of the surface oxygen-containing groups, and Fe^{2+} was completely oxidized to Fe^{3+} by GO and oxygen from the air.¹³ After the addition of $\text{NH}_3\cdot\text{H}_2\text{O}$ (30%), Fe^{3+} was converted to $\text{Fe}(\text{OH})_3$ nanoparticles. Finally, the above solution was subjected to the hydrothermal reduction to produce the $\text{Fe}_2\text{O}_3/\text{N-rGO}$ hydrogel. A possible reaction mechanism for the formation of $\text{Fe}_2\text{O}_3/\text{N-rGO}$ composite is described as follows



SEM images and TEM images show the morphology and the distribution of Fe_2O_3 nanoparticles (Figure 1) of the as-prepared $\text{Fe}_2\text{O}_3/\text{N-rGO}$ composite. From Figure 1a–d, it can be seen that Fe_2O_3 nanoparticles are uniformly distributed on the surface of nitrogen-doped graphene and that $\text{Fe}_2\text{O}_3/\text{N-rGO}$

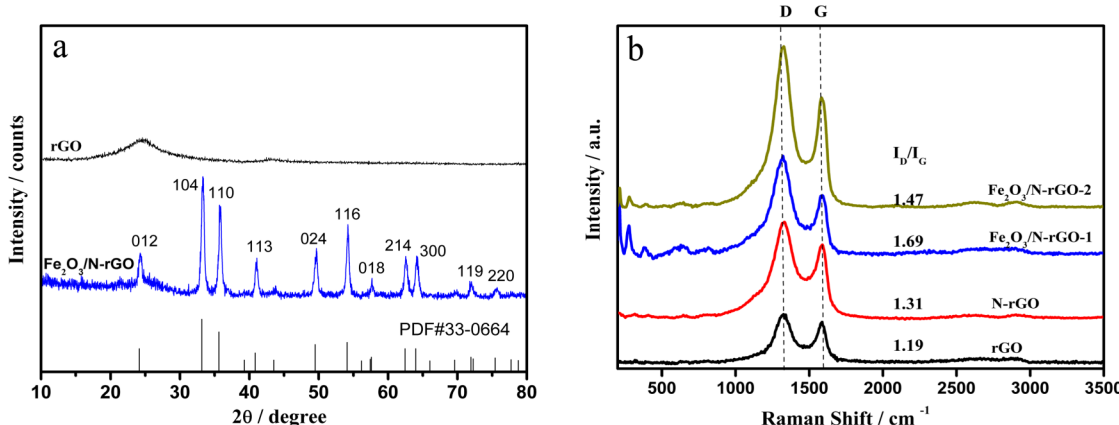


Figure 2. (a) XRD pattern of rGO and the Fe₂O₃/N-rGO composite. (b) The Raman spectra of rGO, N-rGO, and the Fe₂O₃/N-rGO-1 and Fe₂O₃/N-rGO-2 composites.

rGO-2 has a higher density of Fe₂O₃ nanoparticles as a result of the addition of more Fe₂SO₄·7H₂O. TEM images (Figure 1e and f) display the transparent N-rGO and further indicate the size of Fe₂O₃ nanoparticles ranging from 20 to 60 nm. Moreover, there are cubical and rhombic Fe₂O₃ nanoparticles, suggesting the presence of two types of crystals. Besides, the electron diffraction pattern of Fe₂O₃/N-rGO (Figure S1, Supporting Information) shows a concentric ring containing graphene signal and messy electron diffraction spots, indicating that the Fe₂O₃ nanoparticles in the Fe₂O₃/N-rGO composite are polycrystals.

An abundance of structural information and phase identification of the samples can be macroscopically investigated from the XRD pattern. As shown by the XRD pattern of Fe₂O₃/N-rGO in Figure 2a, the major broad peak of N-rGO observed at ~24.4° is shifted from the characteristic 26° for graphite, which corresponds to the (002) diffraction of graphene and the calculated interlayer spacing of 3.59 Å. This value is a little higher than that of common graphene (3.4 Å)^{16–18} due to the presence of residual oxygen-containing functional groups between rGO layers or due to the doped nitrogen atoms. For Fe₂O₃/N-rGO, it exhibits a series of plane peaks, which can respectively be ascribed to (012), (104), (110), (214), (300), (119), and (220) crystal planes of synthesized hematite (JCP DS no. 33-0664). The Fe₂O₃/N-rGO has no other diffraction peaks, demonstrating its high purity and crystallinity. The HRTEM image further confirms the structural information on the Fe₂O₃ particles in the composite. The lattice fringes in a typical HRTEM image (Figure S2a, Supporting Information) are separated by ~2.66 Å, which agrees well with the (104) lattice spacing of the hematite.

The effect of rGO on the disorder degree owing to the nitrogen doping and the introduction of Fe₂O₃ nanoparticles can be characterized by Raman spectra. Figure 2b shows the Raman spectra of the four samples (rGO, N-rGO, Fe₂O₃/N-rGO-1, and Fe₂O₃/N-rGO-2). Two typical Raman peaks of carbon were observed at ~1320 and ~1587 cm⁻¹, which could be assigned to the corresponding D peak and G peak, respectively. D peak is related to the vibrations of sp³ carbon atoms of defects and disorder. The G peak is associated with the vibration of sp² carbon atoms in a graphitic 2D hexagonal lattice. The value of I_D/I_G can be utilized to evaluate the disorder degree in graphene sheets. In Figure 2b, the D peaks are all stronger than the G peaks, suggesting a partially

disordered crystal structure of graphene sheets. It is found that the I_D/I_G ratio of rGO (1.19) is the lowest, indicating the lower disorder degree than others. Subsequently, with the nitrogen-doping, the disorder degree of graphene sheet increases. The growth of Fe₂O₃ nanoparticles on the surface of graphene, both the I_D/I_G ratios of Fe₂O₃/N-rGO-1 and Fe₂O₃/N-rGO-2 increase, suggesting metal oxides can increase the defect and disorder degree of graphene sheet.

The mass ratios of Fe₂O₃ nanoparticles in the composites were evaluated by thermal gravimetric analysis in air. According to the TGA results in Figure 3, the mass ratio of Fe₂O₃ nanoparticles in the composites is 35.1 and 52.0% for Fe₂O₃/N-rGO-1 and Fe₂O₃/N-rGO-2, respectively.

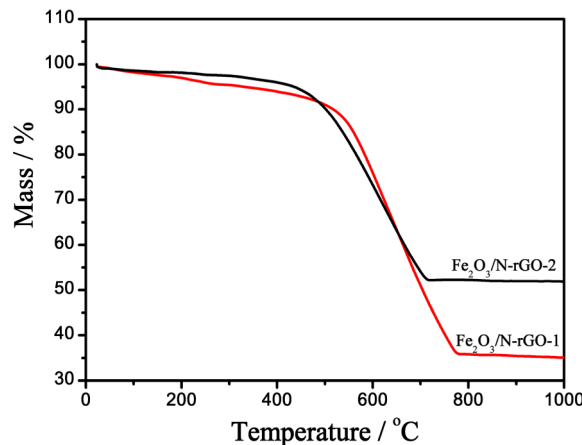


Figure 3. TGA curves of the composites.

XPS was used to evaluate the surface compositions of Fe₂O₃/N-rGO and further to demonstrate the presence of Fe₂O₃. The XPS survey scan of Fe₂O₃/N-rGO (Figure 4a) shows four key elements, C, O, N, and Fe, in the sample. The presence of O and Fe elements confirms the successful deposition of Fe₂O₃ nanoparticles, while the observation of nitrogen with the atom percentage of 6.7% indicates the successful nitrogen doping with the hydrothermal method with ammonia. The high-resolution XPS C 1s spectrum (Figure 4b) is deconvoluted into four subpeaks, indicating the existence of four types of carbon. The peaks at 284.6, 287.7, and 291.0 eV are assigned to C=C/C-C, C=O, and O-C=O. It is noticed that the appearance of the peak at 285.4 eV attributed to C-N confirms the

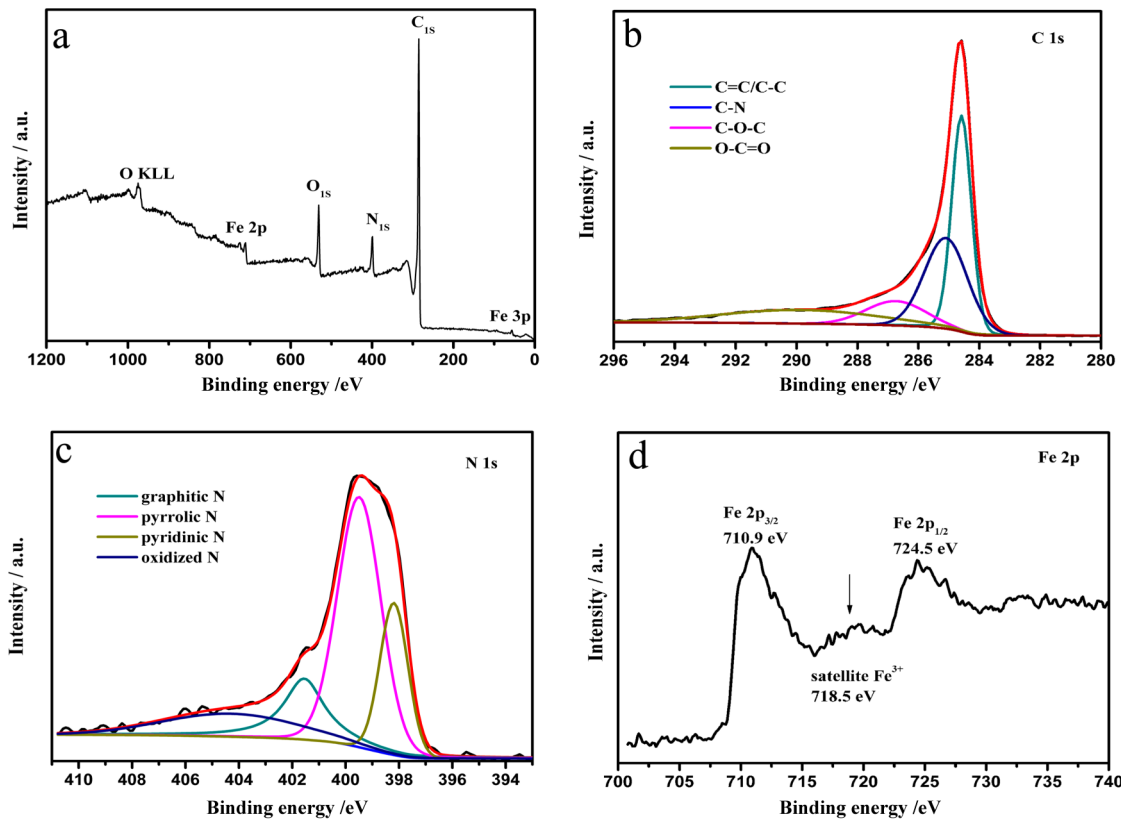


Figure 4. XPS survey scan (a), C 1s spectrum (b), N 1s spectrum (c), and Fe 2p spectrum (d) of $\text{Fe}_2\text{O}_3/\text{N-rGO}$.

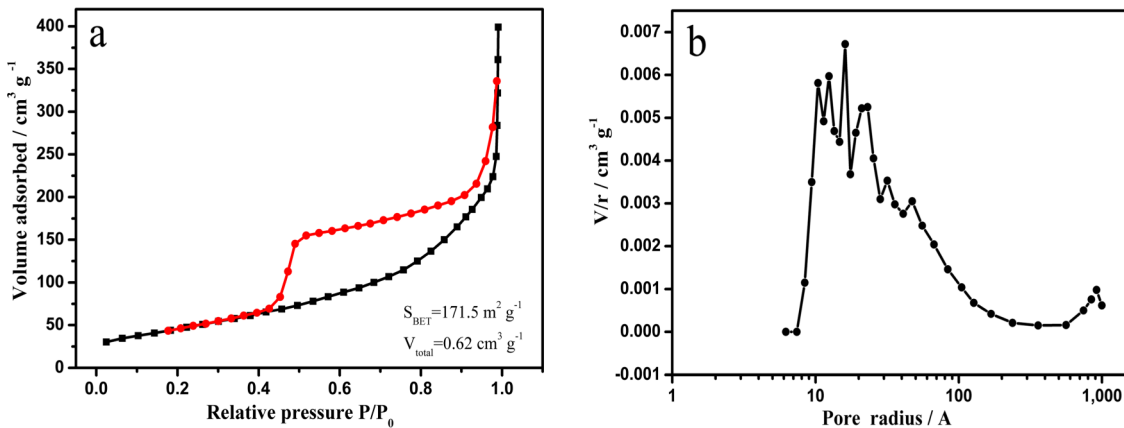


Figure 5. (a) N_2 adsorption–desorption isotherm and (b) pore size distribution of $\text{Fe}_2\text{O}_3/\text{N-rGO}$ at 77 K.

formation of the covalent bonds between graphene sheets and nitrogen.^{19,20} For the XPS N 1s spectrum (Figure 4c), the peaks at 398.1, 399.4, 401.5, and 404.2 eV are assigned to pyridinic N, pyrrolic N, graphitic N, and oxidized N, respectively.²¹ In the Fe 2p spectra (Figure 4d), two distinct peaks located at 710.9 and 724.5 eV are observed and correspond $\text{Fe } 2\text{p}_{3/2}$ and $\text{Fe } 2\text{p}_{1/2}$, which can be utilized to qualitatively determine the ionic states of iron. In addition to these two peaks, the occurrence of a satellite peak at about 718.5 eV is consistent with the characterization of Fe^{3+} .^{22–24}

The nitrogen adsorption–desorption isotherm of $\text{Fe}_2\text{O}_3/\text{N-rGO}$ and the pore size distribution are shown in Figure 5. The curve shows a typical IV characteristic corresponding to the mesoporous structure. A hysteresis loop occurs at a relative pressure of 0.42 and shifts to a higher relative pressure upon

approaching $P/P_0 = 1$, suggesting the presence of macropores (>50 nm in size).²⁵ There exist mainly mesopores and macropores in the sample, which is consistent with the Barrett–Joyner–Halenda (BJH) pore size distribution calculated from the adsorption branch of the nitrogen isotherm. The $\text{Fe}_2\text{O}_3/\text{N-rGO}$ composite with mesopores and macropores is beneficial to improving both the main pseudocapacitance from Fe_2O_3 nanoparticles and the electrochemical double-layer capacitance of N-rGO due to the feasible access of ions in electrolyte to the surface of the electrode through the mesopore pathway. The BET specific surface area and the total pore volume of the sample are $171.5 \text{ m}^2 \text{ g}^{-1}$ and $0.62 \text{ cm}^3 \text{ g}^{-1}$, respectively. However, The BET specific surface area is relatively lower than that of the usual graphene aerogel

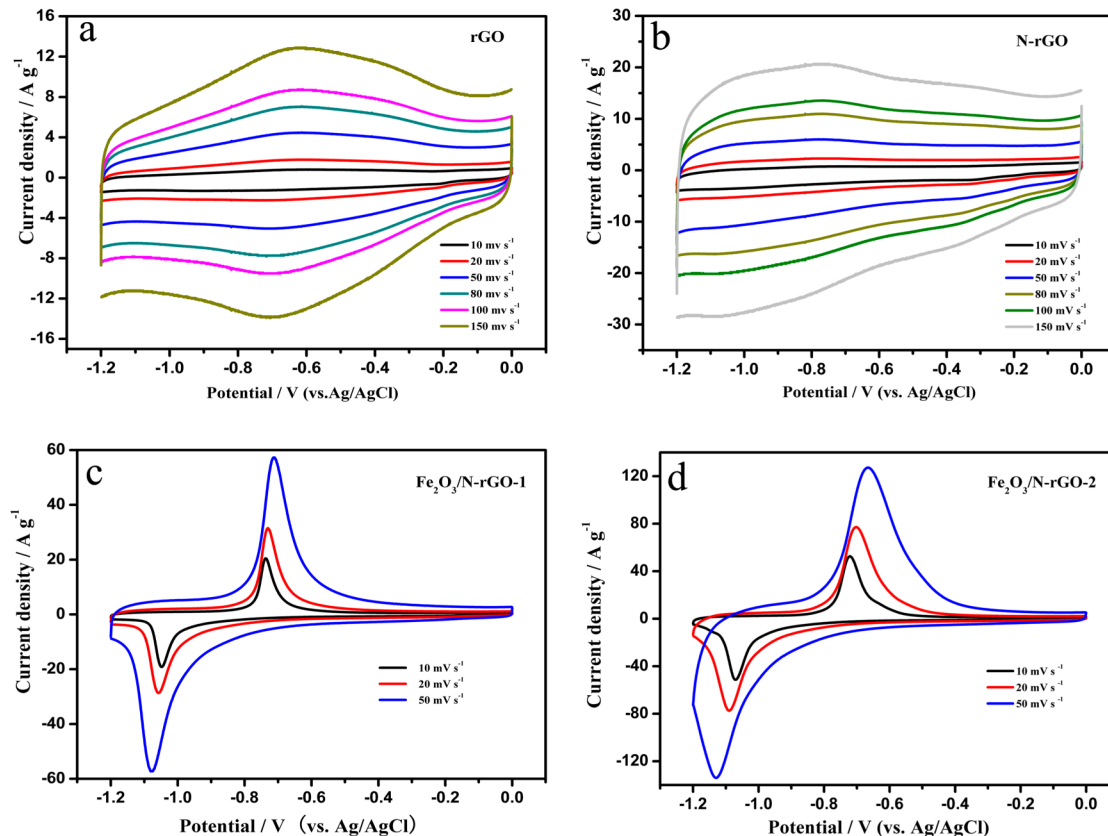


Figure 6. CV curves of (a) rGO, (b) N-rGO, (c) Fe₂O₃/N-rGO-1, and (d) Fe₂O₃/N-rGO-2 at various scan rates.

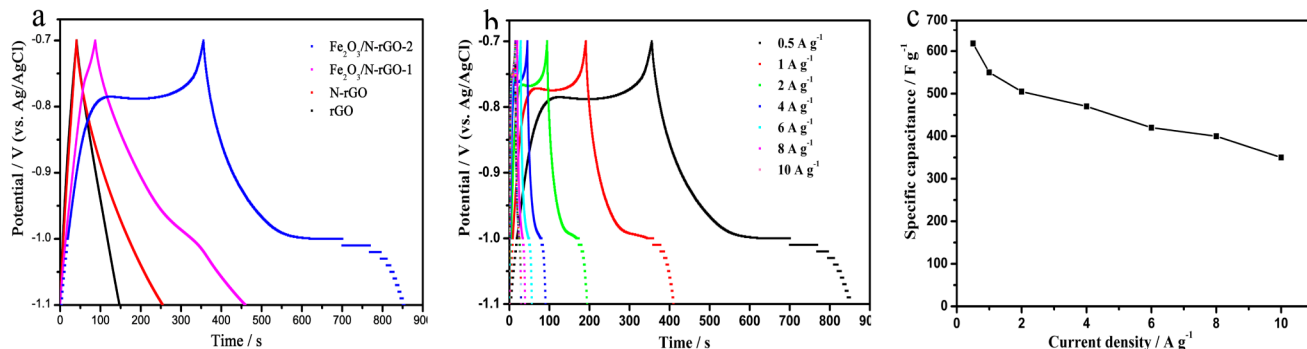


Figure 7. (a) Charge/discharge curves on the electrodes of rGO, N-rGO, Fe₂O₃/N-rGO-1, and Fe₂O₃/N-rGO-2 at a current density of 0.5 A g⁻¹, (b) the charge/discharge curves on the Fe₂O₃/N-rGO-2 electrode at different current densities, and (c) the plot of the specific capacitance of Fe₂O₃/N-rGO-2 against the current densities.

(500–1200 m² g⁻¹),^{26,27} suggesting that the loading of Fe₂O₃ nanoparticles decreases the surface area.^{28–30}

Supercapacitive performances of the electrode materials in the aqueous electrolyte of 1 M KOH are investigated by CV curves in Figure 6. For both rGO and N-rGO, the quasi-rectangular CV curves were observed, indicating that the capacitance mainly originates from the electric double-layer capacitance. Besides, the redox peaks were also observed, ascribed to the pseudocapacitance due to the presence of oxygen-containing groups (for rGO and N-rGO) and doped nitrogen (for N-rGO). By comparing the current response of the CV curves in Figure 6a and b, one can see that N-rGO shows higher capacitance, contributed to by the nitrogen doping with a modified surface and electronic properties. The comparison result indicates that the nitrogen doping could

efficiently improve the capacitive behavior of graphene. Different from the above graphene electrode materials, Fe₂O₃/N-rGO-1 and Fe₂O₃/N-rGO-2 (Figure 6c and d) show one pair of well-defined peaks at about -0.7 V for the anodic scan and -1.1 V for the cathodic scan, which are respectively ascribed to the oxidation and reduction processes of the reversible reaction $\text{Fe}^{2+} \leftrightarrow \text{Fe}^{3+}$.^{31–33} In addition to that, the outstanding peaks arising from the pseudocapacitance of Fe₂O₃ nanoparticles demonstrate that the pseudocapacitance is the major contributor of the capacitance for the composites. It could also be observed that Fe₂O₃/N-rGO-2 shows much higher current response than Fe₂O₃/N-rGO-1 due to the higher Fe₂O₃ mass ratio in the former.

The galvanostatic charge/discharge curves of the rGO, N-rGO, Fe₂O₃/N-rGO-1, and Fe₂O₃/N-rGO-2 with a potential

range of -0.7 to -1.1 V at a current density of 0.5 A g $^{-1}$ are presented in Figure 7a. In the charge/discharge process, rGO and N-rGO show typical triangle curves like other carbon-based electrode materials. For the Fe₂O₃/N-rGO electrode, a charge and a discharge platform occur at around -0.8 (charge step) and -1.0 V (discharge step), which correspond to oxidation and reduction of Fe₂O₃ nanoparticles, respectively. Besides, Fe₂O₃/N-rGO-1 has a shorter plateau than Fe₂O₃/N-rGO-2, which is ascribed to the lower mass ratio of Fe₂O₃ in the composite. The specific capacitances of the electrode materials were calculated from the charge/discharge curves in Figure 7a. The specific capacitance of N-rGO is 267 F g $^{-1}$ at the current density of 0.5 A g $^{-1}$, much higher than that of rGO (132 F g $^{-1}$), indicating the significant role of the nitrogen doping in increasing the capacitance of graphene, which is consistent with the CV characterizations above. More interestingly, the as-prepared Fe₂O₃/N-rGO-2 shows a specific capacitance of 618 F g $^{-1}$ at a charge/discharge current density of 0.5 A g $^{-1}$, indicating a promising potential to be used as the electrode materials in supercapacitors, as shown in Figure 6b. For Fe₂O₃/N-rGO-2, the specific capacitance of 618 F g $^{-1}$ is higher than that of the previously reported Fe₂O₃/graphene.^{34,35} The comparisons of the specific capacitance of Fe₂O₃/N-rGO with other different metal oxide/graphene (MO/G) electrode materials used in the supercapacitor are displayed in detail in Table S1 (Supporting Information). The corresponding energy density is 2.3 , 4.4 , 10.4 , and 13.7 W h kg $^{-1}$ for rGO, N-rGO, Fe₂O₃/N-rGO-1, and Fe₂O₃/N-rGO-2 electrodes, respectively. It is noticed that the energy density values of the Fe₂O₃/N-rGO electrode are several times higher than that of rGO and N-rGO electrodes.

Figure 7b shows the charge/discharge curves of the Fe₂O₃/N-rGO-2 electrode at different current densities, and Figure 7c shows the dependence of the specific capacitance of Fe₂O₃/N-rGO on the discharge current densities. It could be observed that the specific capacitance is still as high as 350 F g $^{-1}$ even at the current density of 10 A g $^{-1}$, indicating that the Fe₂O₃/N-rGO electrode shows a good rate capability.

Electrochemical impedance was utilized to further investigate the role of N-rGO in enhancing the capacitance performance of the composite. Nyquist plots in Figure 8 consist of a semicircle in the high-frequency region and a line in the low-frequency region corresponding to a diffusion process. The EIS data were fitted with NOVA software to the equivalent circuit model, and the parameters are shown in Table 1. R_s , R_{ct1} , C_{dl} , R_{ct2} , and C

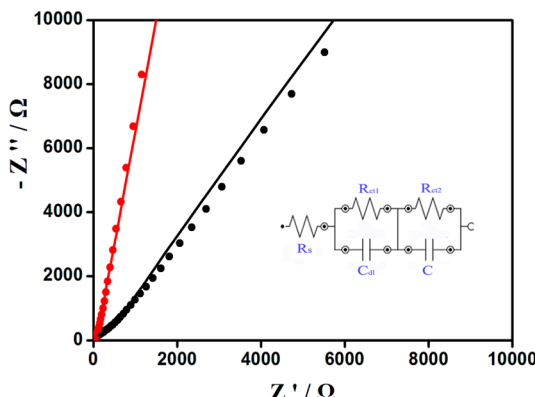


Figure 8. EIS of commercial Fe₂O₃ (black) and the as-prepared Fe₂O₃/N-rGO (red).

Table 1. Parameters Fitted from EIS Spectra

sample	R_s/Ω	R_{ct1}/Ω	$C_{dl}/\mu\text{F}$	$R_{ct2}/\text{k}\Omega$	C/mF
commercial Fe ₂ O ₃	5.48	281	5.22	559	0.401
Fe ₂ O ₃ /N-rGO	4.10	4.65	0.604	68.2	7.79
Fe ₂ O ₃ /N-rGO after the durability testing	3.99	105	10.7	170	1.92

represent the solution resistance, charge-transfer resistance, electrochemical double-layer capacitance, Faradaic charge-transfer resistance, and Faradaic pseudocapacitance, respectively. The R_s of Fe₂O₃/N-rGO is lower than that of commercial Fe₂O₃ (4.10 versus 5.28 Ω). It is suggested that the introduction of N-rGO significantly improves the electrical conductivity of the composite. Moreover, with the introduction of nitrogen, the R_{ct1} and the R_{ct2} decrease, and the C increases, further indicating the synergistic effect between N-rGO and Fe₂O₃ nanoparticles.

Finally, we also examined the durability of the Fe₂O₃/N-rGO-2 electrode for supercapacitor application. The charge/discharge cycle life was measured to evaluate the cycle performance of the Fe₂O₃/N-rGO-2 electrode. As shown in Figure 9a, the specific capacitance of Fe₂O₃/N-rGO-2 is maintained at 56.7% at 4 A g $^{-1}$ after 5000 cycles, indicating that Fe₂O₃/N-rGO shows a good cycling stability. The good electrochemical stability of Fe₂O₃ nanoparticles should be due to the strong interaction between the metal oxide and the graphene bridged by the nitrogen doping.^{36,37} It is noticed that after 5000 cycles, the average particle size of Fe₂O₃/N-rGO in Figure S2b (Supporting Information) did not significantly change except for a slight decline in the number of Fe₂O₃ nanoparticles. Owing to only a little sample loaded on the surface of the glass carbon electrode, the sample was loaded on the carbon felt for cycling and the following XRD measurement (Figure S3, Supporting Information). It is shown that typical diffraction peaks of Fe₂O₃ in the composite are still in existence, whose results are consistent with a morphology change, while the strong signal at around $26^\circ 2\theta$ is mostly contributed to by the carbon from the graphite felt substrate. Electrochemical impedance of the Fe₂O₃/N-rGO electrode before and after 5000 cycles was investigated. As shown in Figure 9b, Nyquist plots are consistent with a semicircle in the high-frequency region and a line in the low-frequency region. The EIS data were fitted to the equivalent circuit model, and the parameters are shown in Table 1. After cycling, the R_s and the C in the Fe₂O₃/N-rGO electrode decrease from 4.10 Ω and 7.79 mF to 3.99 Ω and 1.92 mF, respectively, but the C_{dl} increases. Because the quantity of Fe₂O₃ nanoparticles with poor conductivity in the composite decreases after cycling, the pseudocapacitance from Fe₂O₃ nanoparticles decreases, and the increased mass ratio of N-rGO improves the interface for electrochemical double-layer capacitance and the electrical conductivity between Fe₂O₃ nanoparticles and graphene. On the other hand, a slight decrease of R_s is believed to be evidence that the nitrogen doping could enhance the interaction between the Fe₂O₃ nanoparticle and graphene to enhance its durability.

CONCLUSION

We have successfully prepared Fe₂O₃/N-rGO hydrogels with homodispersed Fe₂O₃ nanoparticles by controlling the growth rate of the nucleus. The size of the Fe₂O₃ nanoparticles is around 20 – 60 nm. The high nitrogen content of 6.7% was incorporated into the graphene support and could significantly

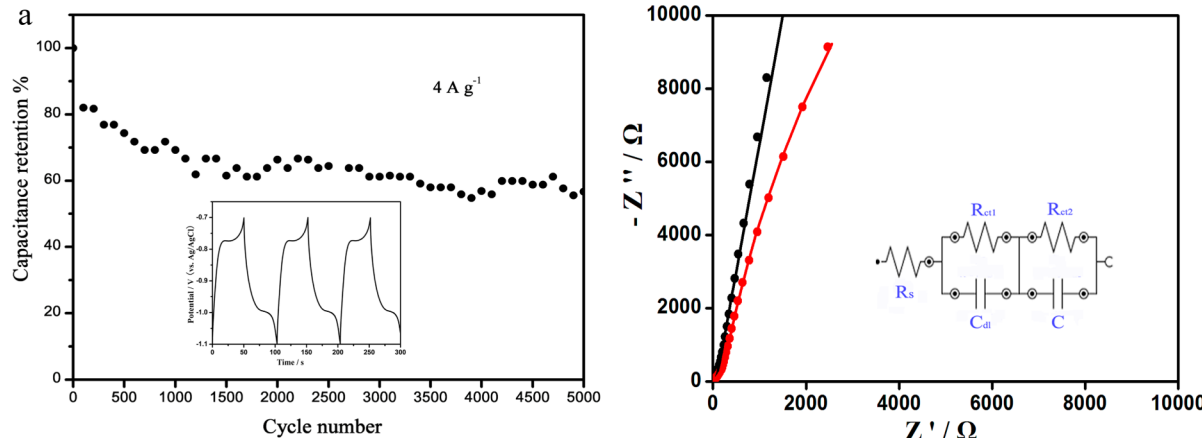


Figure 9. (a) Cycle performance $\text{Fe}_2\text{O}_3/\text{N}-\text{rGO}$ -2 at 4 A g^{-1} for 5000 cycles and (b) EIS spectra of the electrode materials before (black) and after (red) the durability testing.

improve the specific capacitance of graphene (267 F g^{-1} at 0.5 A g^{-1}). The simultaneous deposition of iron oxide into the 3D graphene network shows a positive synergistic effect with the doped nitrogen with respect to the electrochemical capacitance and durability. Nitrogen-doped graphene (N-rGO) increased the electrical conductivity of $\text{Fe}_2\text{O}_3/\text{N}-\text{rGO}$ and played a key role in enhancing the capacitance of the composite. In the charge and discharge process, there is a distinct charge and discharge platform. At a constant discharge current density of 4 A g^{-1} , 56.7% of the initial capacitance still remained after 5000 cycles. The as-prepared $\text{Fe}_2\text{O}_3/\text{N}-\text{rGO}$ by a simple approach shows promising potential as an advanced electrode material for supercapacitors.

ASSOCIATED CONTENT

Supporting Information

Electron diffraction pattern of the $\text{Fe}_2\text{O}_3/\text{N}-\text{rGO}$, HRTEM image of Fe_2O_3 in the $\text{Fe}_2\text{O}_3/\text{N}-\text{rGO}$, TEM of $\text{Fe}_2\text{O}_3/\text{N}-\text{rGO}$, XRD of the $\text{Fe}_2\text{O}_3/\text{N}-\text{rGO}$, and comparisons of the specific capacitance of different metal oxide/graphene (MO/G) electrodes. This material is available free of charge via the Internet at <http://pubs.acs.org>.

AUTHOR INFORMATION

Corresponding Author

*E-mail: shuangyinwang@hnu.edu.cn.

Notes

The authors declare no competing financial interest.

ACKNOWLEDGMENTS

This research was funded by the Marie Curie International Incoming Fellowship Programme of the European Commission and Youth 1000 Talent Program of China

REFERENCES

- Wang, Y.; Xia, Y. Recent Progress in Supercapacitors: From Materials Design to System Construction. *Adv. Mater.* **2013**, *25*, S336–S342.
- Largeot, C.; Portet, C.; Chmiola, J.; Taberna, P.-L.; Gogotsi, Y.; Simon, P. Relation between the Ion Size and Pore Size for an Electric Double-Layer Capacitor. *J. Am. Chem. Soc.* **2008**, *130*, 2730–2731.
- Wang, G.; Zhang, L.; Zhang, J. A Review of Electrode Materials for Electrochemical Supercapacitors. *Chem. Soc. Rev.* **2012**, *41*, 797–828.
- Yu, D.; Wei, L.; Jiang, W.; Wang, H.; Sun, B.; Zhang, Q.; Goh, K.; Si, R.; Chen, Y. Nitrogen Doped Holey Graphene as an Efficient Metal-Free Multifunctional Electrochemical Catalyst for Hydrazine Oxidation and Oxygen Reduction. *Nanoscale* **2013**, *5*, 3457–3464.
- Lightcap, I. V.; Kosel, T. H.; Kamat, P. V. Anchoring Semiconductor and Metal Nanoparticles on a Two-Dimensional Catalyst Mat. Storing and Shuttling Electrons with Reduced Graphene Oxide. *Nano Lett.* **2010**, *10*, 577–583.
- Kamat, P. V. Graphene-Based Nanoarchitectures. Anchoring Semiconductor and Metal Nanoparticles on a Two-Dimensional Carbon Support. *J. Phys. Chem. Lett.* **2009**, *1*, 520–527.
- Wu, S.; Chen, W.; Yan, L. Fabrication of 3D MnO_2 /Graphene Hydrogel for High-Performance Asymmetric Supercapacitor. *J. Mater. Chem. A* **2014**, *2*, 2765–2772.
- Li, Z.; Wang, J.; Liu, S.; Liu, X.; Yang, S. Synthesis of Hydrothermally Reduced Graphene/ MnO_2 Composites and Their Electrochemical Properties as Supercapacitors. *J. Power Sources* **2011**, *196*, 8160–8165.
- Wang, H.; Casalongue, H. S.; Liang, Y.; Dai, H. Ni(OH)₂ Nanoplates Grown on Graphene as Advanced Electrochemical Pseudocapacitor Materials. *J. Am. Chem. Soc.* **2010**, *132*, 7472–7477.
- Bastakoti, B. P.; Oveisi, H.; Hu, C.-C.; Wu, K. C. W.; Suzuki, N.; Takai, K.; Kamachi, Y.; Imura, M.; Yamauchi, Y. Mesoporous Carbon Incorporated with In_2O_3 Nanoparticles as High-Performance Supercapacitors. *Eur. J. Inorg. Chem.* **2013**, *2013*, 1109–1112.
- Xia, X.; Lei, W.; Hao, Q.; Wang, W.; Sun, Y.; Wang, X. One-Pot Synthesis and Electrochemical Properties of Nitrogen-Doped Graphene Decorated with M(OH)_x (M = FeO, Ni, Co) Nanoparticles. *Electrochim. Acta* **2013**, *113*, 117–126.
- Jeong, H. M.; Lee, J. W.; Shin, W. H.; Choi, Y. J.; Shin, H. J.; Kang, J. K.; Choi, J. W. Nitrogen-Doped Graphene for High-Performance Ultracapacitors and the Importance of Nitrogen-Doped Sites at Basal Planes. *Nano Lett.* **2011**, *11*, 2472–2477.
- Yang, P.; Ding, Y.; Lin, Z.; Chen, Z.; Li, Y.; Qiang, P.; Ebrahimi, M.; Mai, W.; Wong, C. P.; Wang, Z. L. Low-Cost High-Performance Solid-State Asymmetric Supercapacitors Based on MnO Nanowires and FeO Nanotubes. *Nano Lett.* **2014**, *14*, 731–736.
- Hu, X.; Yu, J. C.; Gong, J.; Li, Q.; Li, G. α - Fe_2O_3 Nanorings Prepared by a Microwave-Assisted Hydrothermal Process and Their Sensing Properties. *Adv. Mater.* **2007**, *19*, 2324–2329.
- Xue, Y.; et al. Oxidizing Metal Ions with Graphene Oxide: The In Situ Formation of Magnetic Nanoparticles on Self-Reduced Graphene Sheets for Multifunctional Applications. *Chem. Commun.* **2011**, *47*, 11689–11691.
- Liao, K. H.; Mittal, A.; Bose, S.; Leighton, C.; Mkhoyan, K. A.; Macosko, C. W. Aqueous Only Route toward Graphene from Graphite Oxide. *ACS Nano* **2011**, *5*, 1253–1258.

- (17) Wang, G.; Yang, J.; Park, J.; Gou, X.; Wang, B.; Liu, H.; Yao, J. Facile Synthesis and Characterization of Graphene Nanosheets. *J. Phys. Chem. C* **2008**, *112*, 8192–8195.
- (18) Kosynkin, D. V.; Higginbotham, A. L.; Sinitskii, A.; Lomeda, J. R.; Dimiev, A.; Price, B. K.; Tour, J. M. Longitudinal Unzipping of Carbon Nanotubes to Form Graphene Nanoribbons. *Nature* **2009**, *458*, 872–876.
- (19) Han, Z.; Tang, Z.; Li, P.; Yang, G.; Zheng, Q.; Yang, J. Ammonia Solution Strengthened Three-Dimensional Macro-Porous Graphene Aerogel. *Nanoscale* **2013**, *5*, 5462–5467.
- (20) Su, C.; Loh, K. P. Carbocatalysts: Graphene Oxide and Its Derivatives. *Acc. Chem. Res.* **2012**, *46*, 2275–2285.
- (21) Daems, N.; Sheng, X.; Vankelecom, I. F. J.; Pescarmona, P. P. Metal-Free Doped Carbon Materials as Electrocatalysts for the Oxygen Reduction Reaction. *J. Mater. Chem. A* **2014**, *2*, 4085–4110.
- (22) Yamashita, T.; Hayes, P. Analysis of XPS Spectra of Fe^{2+} and Fe^{3+} Ions in Oxide Materials. *Appl. Surf. Sci.* **2008**, *254*, 2441–2449.
- (23) Mou, F.; Guan, J.; Xiao, Z.; Sun, Z.; Shi, W.; Fan, X.-a. Solvent-Mediated Synthesis of Magnetic Fe_2O_3 Chestnut-Like Amorphous-Core/ Γ -Phase-Shell Hierarchical Nanostructures with Strong As(v) Removal Capability. *J. Mater. Chem.* **2011**, *21*, 5414.
- (24) Hyeon, T.; Lee, S. S.; Park, J.; Chung, Y.; Na, H. B. Synthesis of Highly Crystalline and Monodisperse Maghemite Nanocrystallites without a Size-Selection Process. *J. Am. Chem. Soc.* **2001**, *123*, 12798–12801.
- (25) Bavykin, D. V.; Parmon, V. N.; Lapkin, A. A.; Walsh, F. C. The Effect of Hydrothermal Conditions on the Mesoporous Structure of TiO_2 Nanotubes. *J. Mater. Chem.* **2004**, *14*, 3370–3377.
- (26) Worsley, M. A.; Pauzauskie, P. J.; Olson, T. Y.; Biener, J.; Satcher, J. H.; Baumann, T. F. Synthesis of Graphene Aerogel with High Electrical Conductivity. *J. Am. Chem. Soc.* **2010**, *132*, 14067–14069.
- (27) Worsley, M. A.; Olson, T. Y.; Lee, J. R. I.; Willey, T. M.; Nielsen, M. H.; Roberts, S. K.; Pauzauskie, P. J.; Biener, J.; Satcher, J. H.; Baumann, T. F. High Surface Area, sp^2 -Cross-Linked Three-Dimensional Graphene Monoliths. *J. Phys. Chem. Lett.* **2011**, *2*, 921–925.
- (28) Zhang, X.; Sui, Z.; Xu, B.; Yue, S.; Luo, Y.; Zhan, W.; Liu, B. Mechanically Strong and Highly Conductive Graphene Aerogel and Its Use as Electrodes for Electrochemical Power Sources. *J. Mater. Chem.* **2011**, *21*, 6494–6497.
- (29) Zhou, G.; Wang, D.-W.; Li, F.; Zhang, L.; Li, N.; Wu, Z.-S.; Wen, L.; Lu, G. Q.; Cheng, H.-M. Graphene-Wrapped Fe_3O_4 Anode Material with Improved Reversible Capacity and Cyclic Stability for Lithium Ion Batteries. *Chem. Mater.* **2010**, *22*, 5306–5313.
- (30) Chen, W.; Li, S.; Chen, C.; Yan, L. Self-Assembly and Embedding of Nanoparticles by In Situ Reduced Graphene for Preparation of a 3D Graphene/Nanoparticle Aerogel. *Adv. Mater.* **2011**, *23*, 5679–5683.
- (31) Wang, Q.; Jiao, L.; Du, H.; Wang, Y.; Yuan, H. Fe_3O_4 Nanoparticles Grown on Graphene as Advanced Electrode Materials for Supercapacitors. *J. Power Sources* **2014**, *245*, 101–106.
- (32) Du, X.; Wang, C.; Chen, M.; Jiao, Y.; Wang, J. Electrochemical Performances of Nanoparticle Fe_3O_4 /Activated Carbon Supercapacitor Using KOH Electrolyte Solution. *J. Phys. Chem. C* **2009**, *113*, 2643–2646.
- (33) Wu, N.-L.; Wang, S.-Y.; Han, C.-Y.; Wu, D.-S.; Shiue, L.-R. Electrochemical Capacitor of Magnetite in Aqueous Electrolytes. *J. Power Sources* **2003**, *113*, 173–178.
- (34) Wang, D.; Li, Y.; Wang, Q.; Wang, T. Nanostructured Fe_2O_3 –Graphene Composite as a Novel Electrode Material for Supercapacitors. *J. Solid State Electrochem.* **2011**, *16*, 2095–2102.
- (35) Wang, Z.; Ma, C.; Wang, H.; Liu, Z.; Hao, Z. Facilely Synthesized Fe_2O_3 –Graphene Nanocomposite as Novel Electrode Materials for Supercapacitors with High Performance. *J. Alloys Compd.* **2013**, *552*, 486–491.
- (36) Wang, H.; et al. An Ultrafast Nickel–Iron Battery from Strongly Coupled Inorganic Nanoparticle/Nanocarbon Hybrid Materials. *Nat. Commun.* **2012**, *3*, 917.
- (37) Liang, Y.; Wang, H.; Zhou, J.; Li, Y.; Wang, J.; Regier, T.; Dai, H. Covalent Hybrid of Spinel Manganese–Cobalt Oxide and Graphene as Advanced Oxygen Reduction Electrocatalysts. *J. Am. Chem. Soc.* **2012**, *134*, 3517–3523.